Brain shape in human microcephalics and *Homo floresiensis*

Dean Falk*†, Charles Hildebolt‡, Kirk Smith‡, M. J. Morwood§, Thomas Sutikna¶, Jatmiko¶, E. Wayhu Saptomo¶, Herwig Imhof‖, Horst Seidler, and Fred Prior‡**

*Department of Anthropology, Florida State University, Tallahassee, FL 32306; ‡Mallinckrodt Institute of Radiology, Washington University School of Medicine, St. Louis, MO 63110; §Archaeology and Palaeoanthropology, University of New England, Armidale, New South Wales 2351, Australia; ¶Indonesian Centre for Archaeology, Jl. Raya Condet Pejaten No. 4, Jakarta 12001, Indonesia; ‖Clinic for Radiodiagnostics, Medical University of Vienna, A-1090 Vienna, Austria; and **Department of Anthropology, University of Vienna, A-1090 Vienna, Austria

Edited by Marcus E. Raichle, Washington University School of Medicine, St. Louis, MO, and approved December 7, 2006 (received for review October 18, 2006)

Because the cranial capacity of LB1 (*Homo floresiensis*) is only 417 cm^3, some workers propose that it represents a microcephalic *Homo sapiens* rather than a new species. This hypothesis is difficult to assess, however, without a clear understanding of how brain shape of microcephalics compares with that of normal humans. We compare three-dimensional computed tomographic reconstructions of the internal braincases (virtual endocasts that reproduce details of external brain morphology, including cranial capacities and shape) from a sample of 9 microcephalic humans and 10 normal humans. Discriminant and canonical analyses are used to identify two variables that classify normal and microcephalic humans with 100% success. The classification functions classify the virtual endocast from LB1 with normal humans rather than microcephalics. On the other hand, our classification functions classify a pathological *H. sapiens* specimen that, like LB1, represents an ≈3-foot-tall adult female and an adult Basuto microcephalic woman that is alleged to have an endocast similar to LB1's with the microcephalic humans. Although microcephaly is genetically and clinically variable, virtual endocasts from our highly heterogeneous sample share similarities in protruding and proportionately large cerebella and relatively narrow, flattened orbital surfaces compared with normal humans. These findings have relevance for hypotheses regarding the genetic substrates of hominin brain evolution and may have medical diagnostic value. Despite LB1's having brain shape features that sort it with normal humans rather than microcephalics, other shape features and its small brain size are consistent with its assignment to a separate species.

virtual endocast

Microcephaly ("small head") is a condition in which adults typically achieve brain masses of 400–500 g (or cubic centimeters if cranial capacity is used as a surrogate for brain size) and are moderately to severely mentally retarded (1–15). Affected individuals have been reported from all over the world, frequently from consanguineous unions (9, 10, 16–26). Traditionally, the terms "primary microcephaly," "true microcephaly," "microcephaly vera," and "primary autosomal recessive microcephaly" (MCPH, MIM #251200; Online Mendelian Inheritance in Man, www.ncbi.nlm.nih.gov/omim) have been used to describe individuals who were born with abnormally small brains, sloping foreheads, and prominent ears but lacked other "neurological, growth, health, or dysmorphic findings, and [had] no discernible prenatal or postnatal syndrome or cause, such as an aberrant chromosome or structural brain anomaly" (16). [Because MCPH directly affects neurogenesis rather than growth of the skull, some prefer the term "micrencephaly" (27).] MCPH has been distinguished from microcephaly that is acquired or "secondary" to degenerative brain disorders. Since 1998, however, at least seven autosomal recessive microcephalic loci and five associated genes have been identified [see supporting information (SI) Table 2], and all of the general maladies that, by definition, were previously excluded from MCPH have now been observed in one or more affected individuals (see *SI Text*). Variable phenotypes are occasionally correlated with particular kinds of mutations within a given gene [e.g., deletions are generally more severe than duplications (28)] and may be representatives of a continuous phenotype (13, 20, 29). Even the signature sloping forehead of primary microcephalics is occasionally lacking in affected individuals (17, 24) (SI Fig. 4). Primary microcephaly is therefore a genetically and clinically heterogeneous condition that begs the traditional "diagnosis of exclusion" (13, 25, 26, 30).

Given all of this heterogeneity, are there any features other than small size that distinguish microcephalic brains from those of normal humans? To address this question, we compared three-dimensional computed tomographic reconstructions of the internal braincase (virtual endocasts) that reproduce details of external brain morphology, including vessels, sinuses, some sulci, cranial capacities, and shape (1) from a sample of 9 heterogeneous microcephalic humans and 10 normal humans (Fig. 1 and Table 1). Because of the controversial suggestion that LB1 (*Homo floresiensis*) may have been a microcephalic *Homo sapiens* rather than a new species (2–7), we reassessed its virtual endocast in light of our findings. We also assessed the virtual endocasts of a microcephalic woman whose endocast is alleged to resemble that of LB1 (4) and a pathological *H. sapiens* specimen that, like LB1, represents an ≈3-foot-tall adult female. [Although this specimen was labeled as a "dwarf," this heterogeneous medical condition (MCPH, MIM #210710; Online Mendelian Inheritance in Man, www.ncbi.nlm.nih.gov/omim) should not be confused with endemic dwarfism.]

Results

Virtual endocasts were electronically measured to obtain cranial capacities that are traditionally used to approximate brain mass (Table 1). Brain size of microcephalics departs further below normal values as microcephalics mature because it reaches its maximum earlier than is the case for normal humans and then decreases in size (27). For this reason, we estimate the upper limits of brain size for adult microcephalics from data for that group (Michel Hofman, personal communication) rather than using normal humans as a reference population. The mean brain weight for 25 microcephalics (sexes combined) aged 21–74 years

Author contributions: D.F., C.H., and K.S. designed research; D.F., C.H., K.S., M.J.M., T.S., J., E.W.S., H.I., H.S., and F.P. performed research; D.F., C.H., and K.S. analyzed data; and D.F., C.H., K.S., M.J.M., and F.P. wrote the paper.

The authors declare no conflict of interest.

This article is a PNAS direct submission.

Abbreviation: CT, computed tomographic.

†To whom correspondence should be addressed. E-mail: dfalk@fsu.edu.

This article contains supporting information online at www.pnas.org/cgi/content/full/0609185104/DC1.

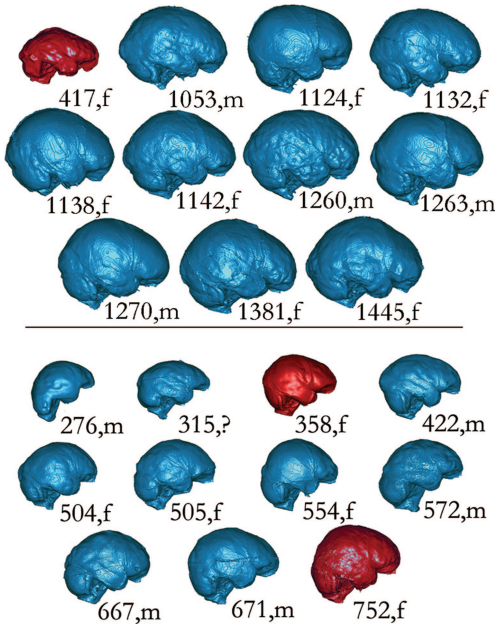

Fig. 1. Comparisons of right lateral views of virtual endocasts from 10 normal humans (*Upper*, blue) and 9 microcephalics (*Lower*, blue). Discriminant and canonical analyses classify the virtual endocast of LB1 [417,f (*Upper*, red)] with normal humans and those from a female human dwarf (752,f, *Lower*) and the Basuto woman (358,f, *Lower*) with microcephalics. Images are labeled with their cranial capacities and sex: f, female; m, male (see Table 1 for details about individual specimens).

is 365 g with a SD of 95 (±3 SD, 80–650 g), which gives an upper limit of 650 g(cm^3) (see *SI Text*). Because this upper limit is considerably higher than the 400–500 g widely quoted as typical for primary microcephalics (9–15), we believe the estimated range is likely to incorporate most, if not all, members of that group. Although two of the microcephalics in our sample have capacities that were slightly above the upper limit, we included them in our initial analyses to increase our sample size (Table 1). One of them (UV 3795, 667 cm^3) was porencephalic (a condition characterized by fluid-filled cavities in the brain) and therefore a secondary microcephalic. The mean capacity for our nine microcephalics is 498 cm^3, and the mean for the seven that have cranial capacities below 650 cm^3 is 450 cm^3. These data suggest the clinically testable hypothesis that adults that are diagnosed as microcephalics and have brain volumes exceeding 650 cm^3 are secondary microcephalics.

Eight measurements were obtained electronically from the virtual endocasts and used to generate four ratios that we thought would discriminate between the two groups {Fig. 2: 2/1 (cerebellar protrusion), [2–4]/1 (relative length posterior base), 6/5 (relative cerebellar width), and 8/6 (relative frontal breadth); see *Materials and Methods*}. Using the four variables, discriminant and canonical analyses were used to study shape differences between microcephalic humans ($n = 9$) and normal humans ($n = 10$), and backward stepwise discriminant analysis was used to select the most powerful discriminators (SI Table 3). All four variables, when analyzed individually, resulted in statistically significant discriminant functions ($P < 0.001$; SI Table 4 and SI Fig. 5). With the resulting classification functions, cerebellar protrusion misclassified one microcephalic as a normal human (SI Table 3). Relative length posterior base misclassified a normal human as a microcephalic. Relative cerebellar width misclassified three microcephalics as normal humans, and relative frontal breadth misclassified two microcephalics as normal humans. The backward stepwise discriminant analysis retained two variables (cerebellar protrusion 2/1 and relative frontal breadth 8/6; SI Tables 3 and 4). Both ratios and the resulting discriminant function (root) were highly significant ($P \leq 0.002$), with the most heavily weighted ratio being cerebellar protrusion. Fig. 3 is a scatter plot of these two variables, which classified microcephalics (M) and normal humans (NH) with 100% success. LB1, the human dwarf, and the Basuto woman (which were not used to develop the discriminant and classification functions) were then classified. LB1 sorted with normal humans (>99% probability) and the other two classified as microcephalics (human dwarf >99% probability and Basuto woman 99% probability; Fig. 3).

When we began our study, we did not know the size or shape of the dwarf's virtual endocast but suspected that the 3-foot-tall specimen might be a microcephalic. The cranial capacity of 752 cm^3 that we obtained for the human dwarf is ≈100 cm^3 above the upper limit we estimate for primary microcephalics. Because the dwarf's brain size is considerably smaller than the mean of ≈1,300 cm^3 for normal women (27) and because our analysis classified the dwarf's brain shape as being that of a microcephalic, we believe it represents a variant of microcephalic primordial dwarfism (MCPH, MIM #210710; Online Mendelian Inheritance in Man, www.ncbi.nlm.nih.gov/omim) and is therefore a secondary microcephalic. LB1's 417-cm^3 endocast, on the other hand, classified with normal humans, indicating that its brain shape differs completely from that of this 3-foot-tall-adult secondary microcephalic female *H. sapiens*.

Because LB1's capacity is only 417 cm^3 (1), we were particularly interested in learning what shape features may discriminate the smaller-brained microcephalics from normal humans. A second analysis was performed after deleting the two microcephalic brains with volumes >650 cm^3 from the data set. The most powerful discriminators from our first analysis (individually and in combination) were, again, used to derive new classification functions, which were used to classify cases. As in the first analysis, cerebellar protrusion misclassified one microcephalic as a normal human. Relative frontal breadth misclassified no case, however, compared with the first analysis in which it misclassified the two largest microcephalics as normal humans. The combination of these two discriminators misclassified no case (with posterior probabilities for group membership exceeding 0.9999 for all cases) and, again, LB1 was classified with normal humans and the dwarf with the microcephalics. When the two big microcephalics were not used to create the classification function, the Basuto woman classified with microcephalics with 100% probability. These data suggest the testable hypothesis that smaller-brained primary microcephalics may have smaller relative frontal breadths than bigger-brained (possibly secondary) microcephalics, and raises the possibility that future research on virtual endocasts and clinical imaging studies could reveal phenotypic characterizations that might have diagnostic significance for known microcephaly loci (SI Table 2) (26).

Discussion

Because the sample of microcephalics we used to develop the classification functions contains only nine individuals, one might argue that it is too small to be representative. As is the case for fossil hominins, microcephalic skulls are rare and our sample has the advantage of being extremely heterogeneous and therefore more likely to capture general features that may characterize microcephaly. Our specimens represent both sexes, ages ranging from 10 years old to adult, cranial capacities from 276 to 671 cm^3, and come from different parts of the world including Europe, the United States, South America, and Africa (Table 1). It contains both primary and secondary microcephalics, although we believe most, if not all, of the individuals below 650 cm^3 are probably primary microcephalics, which is the form of microcephaly most often attributed to LB1. LB1 resembles normal humans in the

Table 1. Specimens used

Specimen	Age, years	Sex	Cranial capacity, cm^3	Repository	ID	Diagnosis	Comments
1	14	M	667	UV	3795*	Secondary microcephaly	Associated with porencephalic, genu valgum, pes calcaneus, scoliosis
2	20–30	M	572	UV	5385	Microcephaly	Skull cast from early 20th century, detailed impressions endocranially
3			315	WU		Microcephaly	
4	10	M	276	AMNH2792a		Primary microcephaly	Skull cast; individual lived in Germany, late 19th century
5	Sub-adult	F	554	PMHU	7200*	Microcephaly	From Peru
6	Adult	M	422	PMHU	7387*	Microcephaly	From Mauritius, African features,
7	Nearly adult	F	504	NMNH	379510*	Microcephaly	From Peru (Chilca)
8	Adult	F	505	UM	96-11-128A	Microcephaly	
9	Adult	M	671	UM	660	Microcephaly	
	32	F	358	FMNH		Microcephaly	Basuto woman, South Africa
	30	F	417	INCA	LB1		*H. floresiensis*
1	25	F	1,138	WU	66-10	Normal human	
2	20–30	M	1,270	FSU	20-30	Normal human	Caucasian
3	40	F	1,132	WU	78-8	Normal human	
4	40	M	1,053	WU	67-11	Normal human	
5	20–30	M	1,263	FSU	C20-C30	Normal human	Caucasian
6	18–25	M	1,260	FSU	C18-C25	Normal human	Caucasian
7	45+	F	1,381	FSU	OBF	Normal human	Black
8	45+	F	1,445	FSU	OFU	Normal human	
9	18–25	F	1,124	FSU	PAAF	Normal human	Probably African-American
10	45+	F	1,142	FSU	001	Normal human	Probably African-American
	20	F	752	UPM	1190*	Dwarf	3 ft tall; Tubingen, Germany

*CT data provided directly; other specimens scanned at Barnes Jewish Hospital, St. Louis. AMNH, Amercian Museum of Natural History; FMNH, Field Museum of Natural History; FSU, Florida State University Department of Anthropology; INCA, Indonesian National Centre for Archaeology, Jakarta; NMNH, National Museum of Natural History (Smithsonian); PMHU, Peabody Museum of Archaeology and Ethnology, Harvard University; UM, University of Michigan Department of Anthropology; UPM, University of Pennsylvania Museum of Archaeology and Anthropology; UV, Museum of Pathology and Anatomy, University of Vienna; WU, Washington University School of Medicine. Data for microcephalics (M) and normal humans (NH) from authors and G. Conroy, Washington University School of Medicine (M#3); K. Mowbray, American Museum of Natural History (M #4); D. Lieberman, Harvard University, M. Morgan and J. Brown, Peabody Museum (M #5–6); Bruno Frohlich and D. Ubelaker, National Museum of Natural History (Smithsonian Institution) (M #7); Milford Wolpoff, University of Michigan (M #8–9); G. Doran and Colette Berbesque, Florida State University (NH #2, 5–10); and Janet Monge, University of Pennsylvania Museum (dwarf). R. Martin provided the endocast of the Basuto woman, upon which we performed a computed tomographic scan.

shape of its orbital surface (Fig. 1 and SI Fig. 6); the endocast of the Basuto (Lesotho) woman that is supposed to resemble LB1 (4, 31) does not (Fig. 1). We are pleased to have obtained a copy of this microcephalic endocast that was described by Martin *et al.* (4, 31) but were unsuccessful at our repeated efforts to obtain information about the repository and specimen number of the key microcephalic endocast that was alleged to be nearly identical to LB1's by Weber *et al.* (2) or, more importantly, to obtain

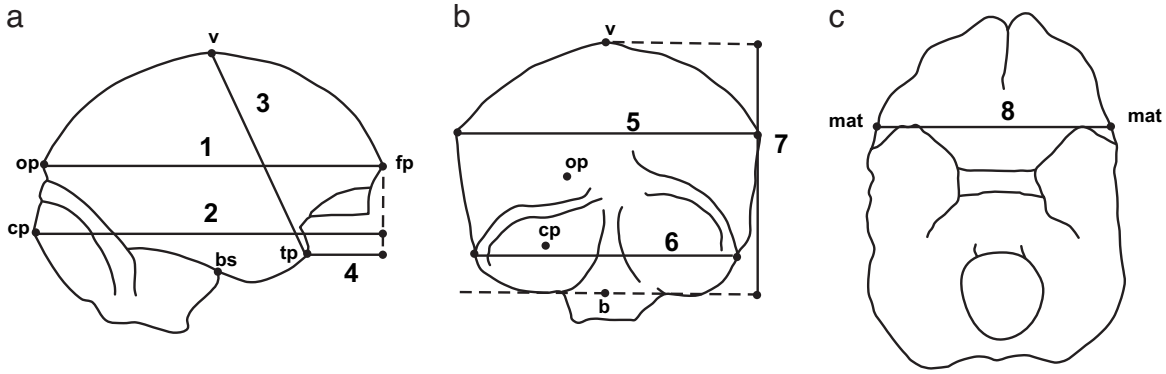

Fig. 2. Key for right lateral (*a*), posterior (*b*), and inferior (*c*) views of endocasts. Measurements (3, a chord; others projected): (*a*) 1, cerebral length (fp-op); 2, cerebellar pole-projected frontal pole; 3, anterior cerebral height (chord v-tp); 4, temporal pole-projected frontal pole; (*b*) 5, cerebral width (right and left points that define maximum projected width); 6, cerebellar width (right and left most lateral points on cerebellum, includes sigmoid sinus if visible in posterior view); 7, endocast height (v-b); (*c*) 8, frontal breadth (mat-mat). Landmarks: b, midpoint on line tangent to the base of cerebellum; bs, intersection of right brainstem with right temporal lobe; cp, most caudal point on the cerebellum in lateral view (may be on either side); fp, most rostral point on the frontal lobes in lateral view (may be on either side); mat, in basal view, point at lateral edge of endocast located at level of the most anterior point of the temporal lobe; op, most caudal point on occipital lobes in lateral view (may be on either side); tp, most rostral point on temporal lobes in lateral view (may be on either side); v, vertex. Four indices used in discriminant and canonical analyses: cerebellar protrusion = 2/1; relative length posterior base = (2–4)/1; relative cerebellar width = 6/5; relative frontal breadth = 8/6.

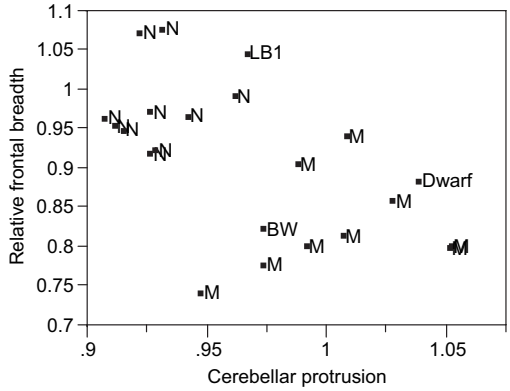

Fig. 3. Scatter plot of relative frontal breadth on cerebellar protrusion. The legend of Fig. 2 contains a description of the measurements that were used to create the ratios. Discriminant analysis demonstrated that these two variables classified microcephalics (M) and normal humans (N) with 100% success. The dwarf, Basuto woman (BW), and LB1, which were not used to develop the classification functions, were classified, respectively, as two microcephalics and a normal human.

a copy or computed tomographic (CT) scan of the endocast so that we might include it in the present analysis.

Our analysis of the virtual endocast of 10-year-old microcephalic Jakob Moegele has been criticized because we performed a computed tomographic scan of a cast whose parts (the calotte and base) were different colors and chemical compositions (4, 31). Despite the skull's calotte and base having been cast separately, the CT data produced a seamless virtual endocast (Fig. 1 and SI Fig. 6) with a volume of 276 cm^3, which is very close to the 272 cm^3 initially reported (32). Indeed, figure 3 of Martin *et al.* (31) reveals the similarity in the shape of the original skull and the cast that we scanned, and shape rather than color of the cast parts is the salient feature in our analyses. Because primary microcephalics are believed to achieve their maximum cranial capacities by around four years of age (27), there is no reason to exclude a 10-year-old microcephalic from our analysis. As noted, the added variation in age and cranial capacity increases the diversity of our sample, which makes it more likely that it captures general traits of microcephalics. The most compelling reason for including Jakob Moegele's virtual endocast in our sample, however, is because our analyses show that it classifies with the other microcephalics in all respects.

Despite the heterogeneity of our microcephalic sample, certain shape features distinguish it from that of normal humans: Microcephalics usually have cerebella that protrude more caudally (Fig. 1 and SI Fig. 4) and appear disproportionately larger than those of normal humans (Fig. 1) (27). The relatively smaller frontal breadths of microcephalics (Fig. 3) are consistent with their typically sloping foreheads, frontal lobes that are more pointed rostrally in dorsal views, and hypothetically smaller forebrains (15, 21, 26, 27, 29). In brains of normal humans, the orbital surface of the frontal lobes (in lateral view) is expanded due to ventral protrusion of the cortex medially (underneath the paths of the olfactory tracts) (33) (Fig. 1 and SI Fig. 4). Virtual endocasts of microcephalics, on the other hand, appear flatter on their orbital surfaces, which is consistent with images of actual brains (21, 29), even when the sulci and gyri appear superficially normal (SI Fig. 4). The indices that describe cerebellar protrusion and relative frontal breadth, which together perfectly sort our sample of microcephalics from normal humans, represent traits that are visually apparent and in keeping with descriptions of microcephalics in the clinical literature. Because our classification functions sort together microcephalic endocasts that range in size from 276–671 cm^3, our shape analyses are not constrained by allometric scaling. (The question of whether microcephalic brains scale allometrically in other ways is beyond the scope of this paper but could be addressed in future studies using 3D geometric morphometrics.)

Two genes that cause microcephaly when mutated (SI Table 2) are hypothesized to have been under pronounced natural selection in the last common ancestor of apes (microcephalin, MCPH1) and in hominins (ASPM, MCPH5) in conjunction with increasing brain size (11, 12, 15) although their precise correlation with phylogenetic increases in this trait has been questioned (25). Our findings are consistent with the hypothesis that genes associated with primary microcephaly may have had a role in primate brain evolution and, more specifically, that some brain dimensions in primary microcephalics resemble those of early hominins (12). Endocasts of an early hominin genus, *Paranthropus*, that is not believed to have been directly ancestral to humans retained an apelike shape of the orbital rostrum (in lateral views) and pointed frontal lobes (in dorsal views) (33) similar to endocasts of primary microcephalics (Fig. 1 and SI Fig. 4). Between 2.5 and 3.0 million years ago, a derived ventrally expanded orbital surface and squared-off frontal lobes (in dorsal view) appeared in another species that may have been directly ancestral to humans, *Australopithecus africanus* (33). These converging data raise the interesting possibility that genes involved in primary microcephaly (e.g., ASPM) may have been important for the evolution of the shape and internal organization of the orbitofrontal cortex in addition to their effects on brain size.

A study that concluded LB1 is a microcephalic pygmy *H. sapiens* rather than a new species of hominin (7) provided no measurements of the neurocranium. This study is refuted not only by our findings but also by an investigation of LB1's affinities using cranial and postcranial metric and non-metric analyses that included comparisons with pygmies from Africa and Andaman Islanders as well as a "pygmoid" excavated from another cave on Flores (34). As shown here, the frontal breadth relative to cerebellar width and lack of cerebellar protrusion of LB1's endocast classify it with 100% probability with normal *H. sapiens* rather than microcephalics. The relative length of its orbital surface also sorts LB1 with *H. sapiens* (1). On the other hand, LB1's endocast shows affinities with *Homo erectus* in its relative height, disparity between its maximum and frontal breadths, relative widths of its caudal and ventral surfaces and long, low lateral profile (1). Its tiny cranial capacity, relative brain size, and derived ventrally expanded orbital surface, however, show affinities with *Australopithecus africanus* (33). Because subsets of LB1's features occur normally in other hominins and because virtual reconstruction adjusted for the slight *in situ* distortion of LB1's skull, these endocast features should not be attributed to pathology nor to postmortem mechanical deformation. The above findings for LB1, plus its bilaterally expanded but otherwise normal-appearing gyri in the region of Brodmann's area 10 (1), are consistent with its attribution to a separate species, *H. floresiensis* (35–37). Although LB1's relative brain size seems not to scale on the ontogenetic curve for *H. erectus* (1), a recent study of brain size in *Pongo* raises the possibility that *H. floresiensis* ' relative brain size may have been reduced because of ecological factors (38), consistent with the insular-dwarfing hypothesis. Other analyses of cranial and postcranial data, however, suggest that *H. floresiensis* may be descended from an earlier small-bodied hominin from either *Australopithecus* or *Homo* (34).

Materials and Methods

CT scans of 5 microcephalic skulls, 1 microcephalic endocast, and 10 normal human skulls (Table 1) were performed at Washington University School of Medicine. The CT scan parameters (and reconstruction kernel) were chosen to produce optimal reconstructions. Our material was scanned with

a Siemens Sensation 64 (Siemens Medical Systems, Erlangen, Germany) clinical multislice, computed-tomography (MCT) scanner, located in Barnes Jewish Hospital (St. Louis, MO). Specimens were aligned along a cranial-caudal axis with the nose facing upward, to simulate a normal anatomical head orientation. Scanning parameters included a 512×512 matrix, 120 kVp, 300 effective mAs, 32 detectors with dual sampling to achieve a 0.6-mm collimation, a 1-sec table increment per gantry rotation, a pitch of 0.8, a reconstruction interval of 0.5 mm, and a H50s reconstruction kernel. With the higher-depth-resolution images that we used, a high-sharpness kernel was unnecessary. Because the features that we identified crossed many planes, our ability to visualize the features was not compromised by the Nyquist frequency (39), which dictates the resolution above which a feature must be sampled to fully reconstruct the feature. All data were archived to compact disk in DICOM format and transferred to a stand-alone workstation for processing. By using commercially available software packages, Mimics 8.11 (Materialise, Ann Arbor, MI) and Analyze 6.1 (Biomedical Imaging Resource, Mayo Clinic, Rochester, MN), the CT image data were visually assessed and inspected for artifacts and damaged areas. CT scans of four additional microcephalic skulls were provided by the Museum of Pathology and Anatomy, University of Vienna (one); Harvard Peabody (two); and the Smithsonian (one) (Table 1). These scans were performed by using our parameters. CT data for a ''female dwarf'' were also provided by the University of Pennsylvania Museum. CT scans of LB1 were performed by using a Siemens Emotion CT scanner in Jakarta and analyzed at the Mallinckrodt Institute of Radiology (1).

Virtual endocasts of all specimens were made by using Mimics 8.11. This software provides tools to convert grayscale CT image data into a wireframe ''virtual'' model. First, the skull is segmented (isolated) from surrounding air and labeled by using a combination of global and local thresholding operations together with a region growing operation. The internal braincase was enclosed, using manual segmentation, to close any contour gaps in the skull, such as at the eye sockets. Once the internal braincase was fully enclosed, as would be done making a traditional latex endocast, the virtual endocast object was defined with a cavity fill operation, and a 3D object was created within the Mimics 3D Object module. This was done by using the high-quality option. By means of the edge extraction tools within the Mimics STL module, a triangulated surface definition was created from the endocast 3D object.

Shape comparisons were performed between the endocasts by using Geomagic Studio 5 software (Raindrop Geomagic, Research Triangle Park, NC).

Each virtual endocast was aligned in dorsal view, and markers were placed on its most rostral frontal pole (fp) and most caudal occipital pole (op). The endocast was then rotated to the right lateral view and a line placed to connect the two markers; the line was rotated to a horizontal position (Fig. 2*A*). The projected fp–op distance in lateral view was measured to obtain cerebral length (measurement 1). In the right lateral view, markers were placed on the vertex (v) and most caudal cerebellar pole (cp). These placements were checked with dorsal and posterior views. In right lateral view, markers were placed on the more rostrally projecting temporal lobe at the middle of its curvature (tp), and the intersection of the right side of the brainstem with the right temporal lobe (bs). Anterior cerebral height (measurement 3) was measured as the direct distance (chord) from vertex to tp; and shortest projected distances were measured from cp and tp to the vertical line tangent to fp (cerebellar pole-projected frontal pole, measurement 2; temporal pole-projected frontal pole, measurement 4). The endocast was then rotated to occipital view (Fig. 2*B*), and markers were added at the most projecting points laterally on both hemispheres of the cerebrum and at the most laterally projecting points of the cerebellum (at the outside edges of the sigmoid sinuses, if visible). These markers were used to measure the projected maximum widths of the cerebrum (cerebral width, measurement 5) and cerebellum (cerebellar width, measurement 6). Endocast height (measurement 7) was measured as the shortest projected distance from vertex to the line tangent to the base of the cerebellum. Frontal breath (measurement 8) was measured at the mean level of the most rostral points on the two temporal poles in basilar view (Fig. 2*C*).

Three months after the baseline measurements were made by K.S. and D.F., all identifying features were removed from the three-dimensional computed tomographic images of the 9 microcephalics and 10 humans and one observer (K.S.) repeated all measurements (T2). Bland-and-Altman plots were used to assess measurement reliability, along with plots of baseline (T1) and repeat (T2) measurements for the microcephalics and normal humans (40). Variance components analyses were used to determine the percentages of variation attributable to subjects and time (baseline and repeated measurements). Measurements of the Basuto woman (8) were made (by K.S.) at the time that repeat measurements were made. Repeatability (reliability) analyses were performed with JMP Statistical Software Release 5.0.1 (SAS Institute, Cary, NC) and MedCalc Statistics for Biomedical Research Version 8.1.0.0 (MedCalc Software, Mariakerke, Belgium). Measurement repeatability was high, with >99% of measurement variability being attributable to subjects (see SI Figs. 7–14).

Discriminant and canonical analyses were used to study shape differences between virtual endocasts of microcephalic humans ($n = 9$) and normal humans ($n = 10$). For these analyses, we used the four ratios that we thought would discriminate between the two groups (2/1, [2–4]/1, 6/5, and 8/6) (Fig. 2). Data were tested for normality with Shapiro–Wilk W tests, and the homogeneity of the variances and covariances was tested with a Box M test. Backward stepwise discriminant analysis was used to select the most powerful discriminators (SI Table 4). For the stepwise procedure, the F to enter was set at 4; F to leave was set at 3; and the tolerance was set at 0.01. Each discriminator plus the combination of the most powerful discriminators was used to classify each case into the group that it most closely resembled. In addition, LB1, the Basuto woman, and a human dwarf (which were not used to develop the discriminant and classification functions) were classified into the two groups. Posterior classification of cases was based on Mahalanobis distances, with *a priori* probabilities being proportional to group sample sizes. Data analyses were performed with JMP Statistical Software Release 5.0.1.2 and STATISTICA (data analysis software system, Version 7.1; StatSoft, Tulsa, OK). Scatter plots for the four variables that were analyzed are presented in SI Fig. 5. The data were normally distributed (Shapiro–Wilk W test, $P > 0.05$), and the variances and covariances were homogeneous across groups (Box M test, $P > 0.05$).

We are deeply grateful to G. Conroy (Washington University School of Medicine), D. Chernoff (Saratoga Imaging), A. Fobbs (National Museum of Health and Medicine), B. Frohlich and D. Ubelaker (National Museum of Natural History, Smithsonian Institution), G. Doran and C. Berbesque (Florida State University), M. N. Haidle (Institute for Prehistory and Early History and Archaeology of the Middle Ages, Tuebingen), M. Hofman (Netherlands Institute for Brain Research), D. Lieberman (Harvard University), R. Martin (Field Museum of Natural History), J. Monge (University of Pennsylvania Museum), M. Morgan and J. Brown (Peabody Museum), K. Mowbray (American Museum of Natural History), L. Sobin (Armed Forces Institute of Pathology), F. Spoor (University College London),

C. Tincher (Barnes Jewish Hospital, St. Louis), R. Wilkinson (Skidmore College), and M. Wolpoff and T. Schoenemann (University of Michigan). This work was supported by National Geographic Society Grants 7769-04 and 7897-05. Acquisition of CT data in Vienna was supported by Austrian Federal Ministry for Culture Science and Education Grant GZ 200.093/I.VI/I/2004.

1. Falk D, Hildebolt C, Smith K, Morwood MJ, Sutikna T, Brown P, Jatmiko, Saptomo EW, Brunsden B, Prior F (2005) *Science* 308:242–245.
2. Weber J, Czarnetzki A, Pusch CM (2005) *Science* 310:236b.
3. Falk D, Hildebolt C, Smith K, Morwood MJ, Sutikna T, Jatmiko, Saptomo EW, Brunsden B, Prior F (2005) *Science* 310:236c.
4. Martin RD, MacLarnon AM, Phillips JL, Dussebieux L, Williams PR, Dobyns WB (2006) *Science* 312:999.
5. Falk D, Hildebolt C, Smith K, Morwood MJ, Sutikna T, Jatmiko, Saptomo EW, Brunsden B, Prior F (2006) *Science* 312:999.
6. Richards GD (2006) *J Evol Biol* 19:1744–1767.
7. Jacob T, Indriati E, Soejono RP, Hsü K, Frayer DW, Eckhardt RB, Kuperavage AJ, Thorne A, Henneberg M (2006) *Proc Natl Acad Sci USA* 36:13421–13426.
8. Dru-Drury EG (1919/1920) *Trans R Soc Afr* 8:149–154.
9. Jackson AP, Eastwood H, Bell SM, Adu J, Toomes C, Carr IM, Roberts E, Hampshire DJ, Crow YJ, Mighell AJ, *et al.* (2002) *Am J Hum Genet* 71:136–142.
10. Kumar A, Markandaya M, Girimaji SC (2002) *J Biosci* 27:629–632.
11. Zhang J (2003) *Genetics* 165:2063–2070.
12. Evans PD, Anderson JR, Vallender EJ, Choi SS, Lahn BT (2004) *Hum Mol Genet* 13:1139–1145.
13. Verloes A (2004) *Orphanet*, www.orpha.net/data/patho/GB/uk-MVMSG.pdf.
14. Evans PD, Gilbert SL, Mekel-Bobrov N, Vallender EJ, Anderson JR, Vaez-Azizi LM, Tishkoff SA, Hudson RR, Lahn BT (2005) *Science* 309:1717–1720.
15. Gilbert SL, Dobyns WB, Lahn BT (2005) *Nat Rev Genet* 6:581–590.
16. Bond J, Scott S, Hampshire DJ, Springell K, Corry P, Abramowicz MJ, Mochida GH, Hennekam RCM, Maher ER, Fryns J-P, *et al.* (2003) *Am J Hum Genet* 73:1170–1177.
17. Jackson AP, McHale DP, Campbell DA, Jafri H, Rashid Y, Mannan J, Karbani G, Corry P, Levene MI, Mueller RF, *et al.* (1998) *Am J Hum Genet* 63:541–546.
18. Moynihan L, Jackson AP, Roberts E, Karbani G, Lewis I, Corry P, Turner G, Mueller RF, Lench NJ, Woods CG (2000) *Am J Hum Genet* 66:724–727.
19. Pattison L, Crow YJ, Deeble VJ, Jackson AP, Jafri H, Rashid Y, Roberts E, Woods CG (2000) *Am J Hum Genet* 67:1578–1580.
20. Jamieson CR, Fryns J-P, Jacobs J, Matthijs G, Abramowicz MJ (2000) *Am J Hum Genet* 67:1575–1577.
21. Peiffer A, Singh N, Leppert M, Dobyns WB, Carey JC (1999) *Am J Med Genet* 84:137–144.
22. Kelley RI, Robinson D, Puffenberger EG, Strauss KA, Morton DH (2002) *Am J Med Genet* 112:318–326.
23. Rosenberg MJ, Agarwala R, Bouffard G, Davis J, Fiermonte G, Hilliard MS, Koch T, Kalikin LM, Makalowska I, Morton DH, *et al.* (2002) *Nat Genet* 32:175–179.
24. Roberts E, Hampshire DJ, Pattison L, Springell K, Jafri H, Corry P, Mannon J, Rashid Y, Crow Y, Bond J, *et al.* (2002) *J Med Genet* 39:718–721.
25. Woods CG, Bond J, Enard W (2005) *Am J Hum Genet* 76:717–728.
26. Mochida GH, Walsh CA (2001) *Curr Opin Neurol* 14:151–156.
27. Hofman MA (1984) *J Neurol* 231:87–93.
28. Brewer C, Holloway S, Zawalnyski P, Schinzel A, FitzPatrick D (1998) *Am J Hum Genet* 63:1153–1159.
29. Trimborn M, Bell SM, Felix C, Rashid Y, Jafri H, Griffiths PD, Neumann LM, Krebs A, Reis A, Sperling K, *et al.* (2004) *Am J Hum Genet* 75:261–266.
30. Dobyns WB (2002) *Am J Med Genet* 112:315–317.
31. Martin RD, Maclarnon AM, Phillips JL, Dobyns WB (2006) *Anat Rec* 288A:1123–1145.
32. Vogt C (1867) *Arch Anthropol* 2:129–284.
33. Falk D, Redmond JC, Jr, Guyer J, Conroy GC, Recheis W, Weber GW, Seidler H (2000) *J Hum Evol* 38:695–717.
34. Argue D, Donlon D, Groves C, Wright R (2006) *J Hum Evol* 51:360–374.
35. Brown P, Sutikna T, Morwood MJ, Soejono RP, Jatikmo, Saptomo WW, Due RA (2004) *Nature* 431:1055–1061.
36. Morwood MJ, Soejono RP, Roberts RG, Sutikna T, Turney CSM, Westaway KE, Rink WJ, Zhao J-X, van den Bergh GD, Due RA, *et al.* (2004) *Nature* 431:1087–1091.
37. Morwood MJ, Brown P, Jatikmo, Sutikna T, Saptomo EW, Westaway KE, Due RA, Roberts RG, Maeda T, Wasisto S, Djubiantono T (2005) *Nature* 437:1012–1017.
38. Taylor AB, van Schaik CP (2007) *J Hum Evol* 52:59–71.
39. Dainty JC, Shaw R (1974) *Image Science: Principles, Analysis and Evaluation of Photographic-type Imaging Processes* (Academic, New York).
40. Altman DG, Bland JM (1983) *Statistician* 32:307–317.